Joule

CellPress

Article

Design principles for zero-strain Li-ion cathodes

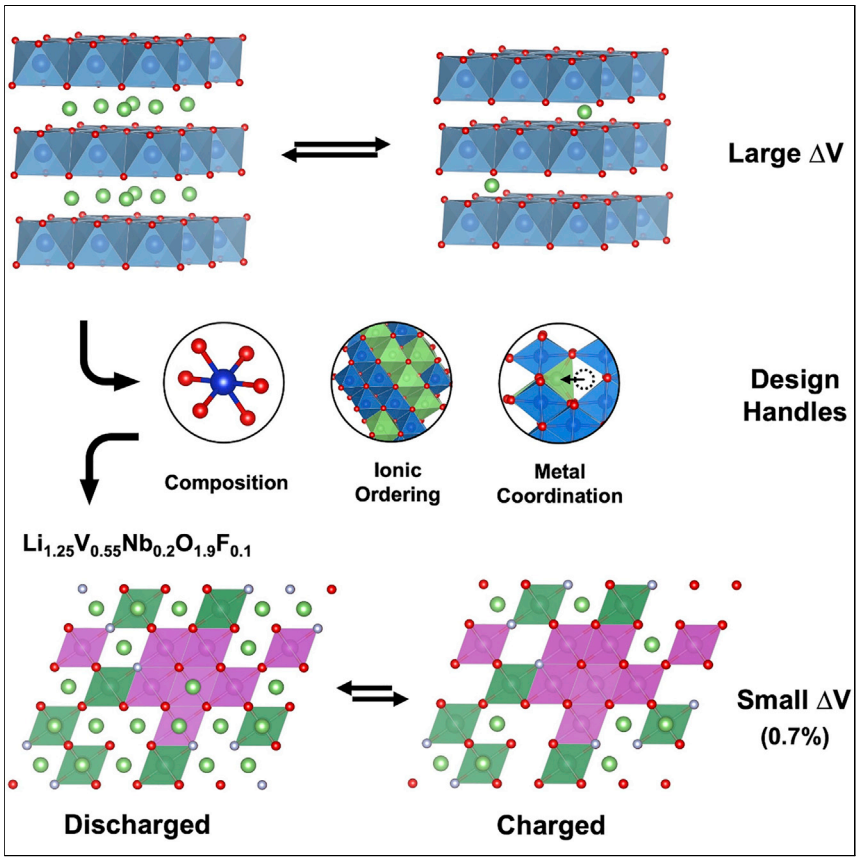

The development of safe and scalable solid-state batteries has been hindered by the large volume change during the electrochemical cycling of cathode materials, which causes complex chemo-mechanical degradation at the electrode-electrolyte interface. Combining theory and experiment, we have established chemical composition, ionic ordering, and metal coordination as three major factors that influence the volume change in cathode structures. Guided by these insights, we synthesized disordered rocksalt cathodes that undergo quasi-zero volume change upon cycling.

Xinye Zhao, Yaosen Tian, Zhengyan Lun, Zijian Cai, Tina Chen, Bin Ouyang, Gerbrand Ceder

bouyang@berkeley.edu (B.O.)
gceder@berkeley.edu (G.C.)

Highlights

Theory-guided synthesis of Li-ion cathode with nearly zero volume change upon charge

Composition, ionic ordering, and local cation coordination affect volume change

V–Nb Li-excess disordered rocksalt compounds exhibit excellent structural stability

Zhao et al., Joule 6, 1–18
July 20, 2022
https://doi.org/10.1016/j.joule.2022.05.018

Please cite this article in press as: Zhao et al., Design principles for zero-strain Li-ion cathodes, Joule (2022), https://doi.org/10.1016/j.joule.2022.05.018

Joule

CellPress

Article

Design principles for zero-strain Li-ion cathodes

Xinye Zhao,[1,2] Yaosen Tian,[1,2] Zhengyan Lun,[1,2] Zijian Cai,[1,2] Tina Chen,[1,2] Bin Ouyang,[1,2,*] and Gerbrand Ceder[1,2,3,*]

SUMMARY

The cycling of cathode materials for Li-ion batteries is often accompanied by a change in volume, posing a challenge to the integrity of cathode particles and electrolyte/cathode interface in solid-state batteries. To enhance capacity retention, it is thus crucial to design materials that remain structurally invariant during electrochemical cycling. Here, we use well-calibrated first-principles calculations to systematically investigate the effect of transition-metal chemistry, cation ordering, Li site occupancy, redox-inactive species, anion substitution, and cation migration on the volume change associated with the delithiation of cathode materials with an FCC anion framework. Suggested by an in-depth first-principles Monte Carlo simulation of the Li^{+}–V^{3+}–Nb^{5+}–O^{2-}–F^{-} system, we experimentally confirm $Li_{1.3}V_{0.4}Nb_{0.3}O_2$ and $Li_{1.25}V_{0.55}Nb_{0.2}O_{1.9}F_{0.1}$ as nearly zero-strain cathodes. Our study establishes a fundamental understanding of the important physical descriptors that determine the dimensional change of materials during cycling and provides general guidelines for designing low- or zero-strain cathodes.

INTRODUCTION

The continued improvement in the performance of Li-ion batteries (LIBs) has made them the technology of choice for electrical energy storage. LIBs are now the only rechargeable battery other than lead-acid batteries that have an annual production rate of >5 GWh $year^{-1}$, and this rate is expected to reach hundreds of GWh $year^{-1}$ over the next 5 years. Current commercial cathodes undergo a significant volume change when Li is cycled in and out of them. For example, layered $LiNi_{0.8}Co_{0.1}Mn_{0.1}O_2$ (NCM811) experiences a volume decrease of ~6% when charged to 4.4 V.[1] Spinel $LiMn_2O_4$ undergoes a lattice-parameter contraction of more than 3% when charged to 4.5 V,[2] corresponding to a volume change of more than 9%. $LiFePO_4$ contracts by 6%–7% when charged to $FePO_4$.[3,4] The volume change of a cathode material can be detrimental in many ways. Any non-homogeneity of the strain, either inside cathode particles or within the composite cathode, leads to mechanical stresses that can degrade the primary and secondary particles, especially at high states of charge (SOCs).[5] The microcracks and fractures accumulated in the cathode particles create fresh surfaces without protection from a stable electrolyte–cathode interface, resulting in capacity fading over long-term cycling. Volume changes at the electrode level can also lead to progressive damage to the separator and even catastrophic failure.[6] In solid-state batteries (SSBs), problems caused by the volume change of the active cathode material are considerably aggravated. "Breathing" cathodes push the surrounding solid electrolyte away,[1,7] creating a substantial challenge to long-term capacity retention because of cathode/solid-electrolyte contact loss, coating breakdown, and

Context & scale

Cathode materials for Li-ion batteries commonly suffer from chemo-mechanical structural degradation during cycling. The repeated (de-)lithiation processes induce severe volume change and deteriorate the structural integrity of the cathode particles and cathode coatings. For solid-state batteries, this is particularly detrimental as the solid electrolyte lacks the mechanical compliance to accommodate the local expansion and contraction of the cathode particles, resulting in cathode-electrolyte decohesion, increasing cell impedance, and capacity loss. Here, we demonstrate a well-calibrated computational approach to evaluate the structural and compositional factors that determine the volume change of cathodes upon charge and experimentally validate our predictions. Our work establishes guidelines for designing novel cathodes with high dimensional stability for next-generation batteries.

Please cite this article in press as: Zhao et al., Design principles for zero-strain Li-ion cathodes, Joule (2022), https://doi.org/10.1016/j.joule.2022.05.018

pressure changes in a volume-constrained cell environment.[8–11] It would therefore be transformative to establish zero-strain (zs) cathodes that exhibit small or even zero volume change upon Li extraction or insertion. In this work, we provide a quantitative and actionable analysis of the structural and chemical factors that contribute to volume change and integrate them into the design of two near-zs materials.

Although $Li_4Ti_5O_{12}$ (LTO) is well known as a zs anode material,[12,13] limited experimental effort has been devoted to developing zs cathode materials. In 2017, de Biasi et al. demonstrated that by tuning the Ni/Co/Mn ratio in layered $LiNi_xCo_yMn_zO_2$ (NCM, with $x + y + z = 1$) compounds, one could reduce the volume change below a specific SOC.[14] However, an initial anisotropic structural contraction followed by an expansion is still observed in such layered cathodes throughout the delithiation process. Disordered rocksalt Li-excess (DRX) compounds, which share their face-centered cubic (FCC) anion framework with well-established layered and spinel cathode materials, are cubic due to the cation disorder and are some of the first cathode materials for which a very small and isotropic volume change has been demonstrated.[15–17] In 2014, Lee et al. developed a Cr–Mo-based DRX material (formed *in situ* from a layered structure after 5–10 cycles) that exhibits a near-zero volume change of ~0.12% when charged up to 4.3 V.[15] In 2017, Yabuuchi and co-workers similarly demonstrated that V-containing DRX materials could also exhibit a small dimensional change when charging.[16,17]

In this work, we investigate the role of the compositional and structural factors that control the volume change upon Li removal: the choice of redox-active transition-metal (TM) species, the nature of Li–TM cation ordering, Li occupancy in tetrahedral versus octahedral sites, TM migration, presence of redox-inactive metals, and amount of F substitution for oxygen. *Ab initio* computations are used to investigate the effect of each factor separately in order to establish general design rules for zs cathode materials. Our work leads to precise and generalizable insights into volume change upon delithiation: We observe that cathode materials based on the redox of early TM ions with only electrons in t_{2g} orbitals generally undergo a smaller volume change upon (de-)lithiation. Moreover, a cubic intercalation host removes the anisotropy of the volume expansion/contraction and is also found to reduce its magnitude. Migration of Li from octahedral to tetrahedral sites as Li is removed from the structure can also reduce volume contraction upon charging, as does TM migration into the tetrahedral site at the end of charge.

Following these design principles, we investigated the Li^+–V^{3+}–Nb^{5+}–O^{2-}–F^- (LVNOF) DRX compositional space to find specific compositions that undergo minimal volume change upon delithiation. We predict and synthesize $Li_{1.3}V_{0.4}Nb_{0.3}O_2$ (LVNO43) and $Li_{1.25}V_{0.55}Nb_{0.2}O_{1.9}F_{0.1}$ (LVNOF552) as nearly "zs" compositions. In particular, the fluorinated LVNOF552 exhibits a maximum isotropic volume change of ~0.7% over a capacity of 200 mAh/g. It has a volume difference of only 0.9 $Å^3$/Li between the 1.5 V discharged and 4.8 V charged state. Our work establishes a comprehensive understanding of how structural and compositional factors affect the volume change of FCC anion-based cathode materials and provides a quantitative framework to design zs cathode candidates.

RESULTS

Effects of TM chemistry, cation ordering, and Li occupancy

DFT calculations were performed using the SCAN+rVV10 functional.[18] This approach has been proven to be more accurate than GGA or GGA+*U* for geometry

[1]Department of Materials Science and Engineering, University of California, Berkeley, Berkeley, CA 94720, USA

[2]Materials Sciences Division, Lawrence Berkeley National Laboratory, Berkeley, CA 94720, USA

[3]Lead contact

*Correspondence: bouyang@berkeley.edu (B.O.), gceder@berkeley.edu (G.C.)

https://doi.org/10.1016/j.joule.2022.05.018

Please cite this article in press as: Zhao et al., Design principles for zero-strain Li-ion cathodes, Joule (2022), https://doi.org/10.1016/j.joule.2022.05.018

and structure selectivity as it considers intermediate-to-long-range van der Waals interactions.[18,19] To assess the validity of this approach for typical battery chemistries and structures, we benchmarked the performance of GGA+*U*, SCAN, and SCAN+rVV10 in predicting the unit-cell volume of various oxide materials with an O3-layered structure (R-3m space group) against experimental data. As shown in Table S1, compared with GGA+*U*, SCAN+rVV10 yields much more accurate volumes for the layered compounds, with GGA+*U* tending to overestimate the volume.[20] SCAN and SCAN+rVV10 have on average similar accuracy for lithiated TM oxides; however, SCAN overestimates the unit-cell volume of the fully delithiated structure (CoO_2) and fails to capture the volume decrease associated with the extraction of Li. We therefore chose the SCAN+rVV10 functional to properly evaluate the volume change associated with Li extraction in metal oxides.

Our approach, enabled by *ab initio* computing, is to isolate each chemical and structural factor by keeping as much as possible all other factors unchanged when comparing volume changes. Although volume change is most often quoted as a percentage change of the unit cell (independent of the capacity), we argue here that a more meaningful quantity can be achieved by normalizing the volume change by the amount of capacity cycled. This removes focus from systems that solely have small volume change because they have small capacity. In thermodynamics, the relevant quantity is the partial molar volume of Li in the compound, defined as the derivative of the volume with respect to Li content (Equation 1). In most of our calculations, we approximate the partial molar volume of Li as the finite difference of the volumes of the lithiated and delithiated states normalized by the amount of Li removed:

$$\overline{V}_{\mathrm{Li}} = \left(\frac{\partial V}{\partial n_{\mathrm{Li}}}\right)_{T,P,n_{j\neq \mathrm{Li}}} \approx \frac{(V_{\mathrm{d}} - V_{\mathrm{l}})}{n_{\mathrm{Li,d}} - n_{\mathrm{Li,l}}}, \qquad \text{(Equation 1)}$$

where V_{d} and V_{l} are, respectively, the volumes of the delithiated and lithiated structures, and n_{Li} is the number of Li atoms present in the structure. Consistent with the thermodynamic interpretation, the partial molar volume of Li in a compound can be thought of as the volume that Li occupies. In this work, we calculate and analyze the negative partial molar volume of Li ($-\overline{V}_{\mathrm{Li}}$), which we call the partial molar extraction volume of Li to make it more consistent with how the battery field discuss volume effects.

We use four common $LiMO_2$ structure types to evaluate volume changes: The O3-layered structure, lithiated $Li_2M_2O_4$ spinel, the γ-$LiFeO_2$-type ordered structure, and a cation-disordered rocksalt. We evaluate the volume change of each structure with multiple TMs, even when that creates a compound which may not be the most stable structure for that chemistry so that the effect of structure and TM can be fully isolated.

The calculated partial molar extraction volume of Li for the O3-layered $LiMO_2$ structures with varying TM is shown in Figure 1. The electronic configuration of each TM cation is also provided along the x axis. In layered materials, as in other rocksalt-derived compounds, each TM is octahedrally coordinated with its first nearest neighbor O anions forming a $(TM)O_6$ unit.[21] As a result, the *d*-orbitals split into three lower-energy t_{2g} and two higher-energy e_g orbitals.[22] TMs with only t_{2g} electrons are colored blue, whereas those that also have e_g electrons are colored in aquamarine.

The results in Figure 1 indicate that although all the investigated layered materials undergo a volume decrease upon full delithiation, cations with only t_{2g} electron occupancy, such as Ti^{3+}, V^{3+}, Cr^{3+}, and Co^{3+}, generally lead to a smaller volume

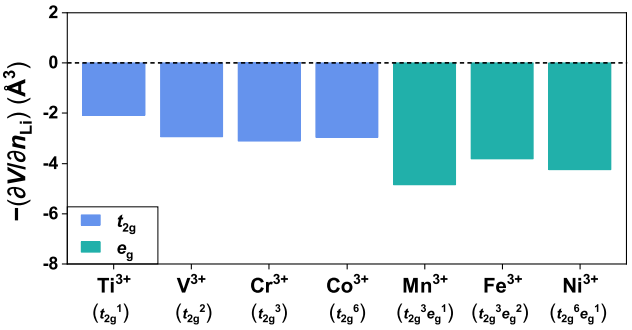

Figure 1. Effect of redox chemistry

Calculated partial molar extraction volume of Li of O3-layered $LiMO_2$ with notation on the corresponding electronic structure of TM^{3+}.

See also Figure S1.

change, with Ti^{3+} and V^{3+} having the lowest magnitude $-\overline{V}_{Li}$ of −2.08 and −2.94 Å^3. In contrast, $LiMnO_2$ and $LiNiO_2$, which have redox TMs with electrons occupying e_g orbitals, undergo larger volume change, with $-\overline{V}_{Li}$ of −4.85 and −4.25 Å^3. These results implicate a correlation between chemistry, namely the *d*-orbital occupancy of the TM species, and volume change upon delithiation in layered materials. It is interesting that O3-$LiFeO_2$ also exhibits a relatively small $-\overline{V}_{Li}$ of −3.81 Å^3 upon the removal of all Li, despite Fe^{3+} having an e_g electronic configuration. We will discuss the reasons for this phenomenon which is related to the Jahn-Teller (JT) activity of Fe^{4+} in a later section. To corroborate the trend of volume change with chemistry, we also show the computed volume of Li extraction in layered structures with O1 stacking in Figure S1A, which shows similar behavior to the O3-compounds. The small volume change associated with the oxidation of a t_{2g} state is also observed in O3-compounds with 4*d* and 5*d* TM ions, as shown in Figure S1D.

To examine the effect of cation arrangement, we calculated the partial molar extraction volume of Li in three structures with FCC-like cation packing: O3-layered, lithiated spinel, and γ-$LiFeO_2$ ordering. For easier comparison, we visualize these three cation orderings within the same cell shape in Figure 2A. Note that the lithiated spinel is the LT-$Li_2Co_2O_4$ structure with only octahedral cation occupancy.[23] Because of the overlithiation no tetrahedral occupancy is present in this structure, although the cations have the same ordering as in LiM_2O_4 spinels. We note that the spinel-like $LiFeO_2$ structures were calculated using the GGA+*U* (U_{Fe} = 4.0 eV) functional instead of SCAN+rVV10, as the latter fails to correctly produce the high-spin state of Fe^{4+} and its associated JT activity. The calculated $-\overline{V}_{Li}$ for each structure is plotted in Figure 2B. Among the three polymorphs considered, the layered structure generally exhibits the largest partial molar extraction volume of Li. In contrast, Li removal causes less volume change in the lithiated spinel and γ-$LiFeO_2$ structures.

We speculate that it is the more isotropic ordering of Li/TM in the lithiated spinel and γ-$LiFeO_2$ host structures that gives them a comparatively lower volume reduction upon delithiation. If that is the case, a cation-disordered structure would similarly exhibit low volume contraction, given its isotropic ordering.[15,24] To confirm this speculation, we investigated the volume change in a disordered rocksalt structure that was generated by swapping the 3a Li ions randomly with the 3b TM ions from the 3 × 3 × 1 O3-layered supercells. In total, 34 random structures were generated for each chemistry to obtain reasonable statistics. For each chemistry, we took the

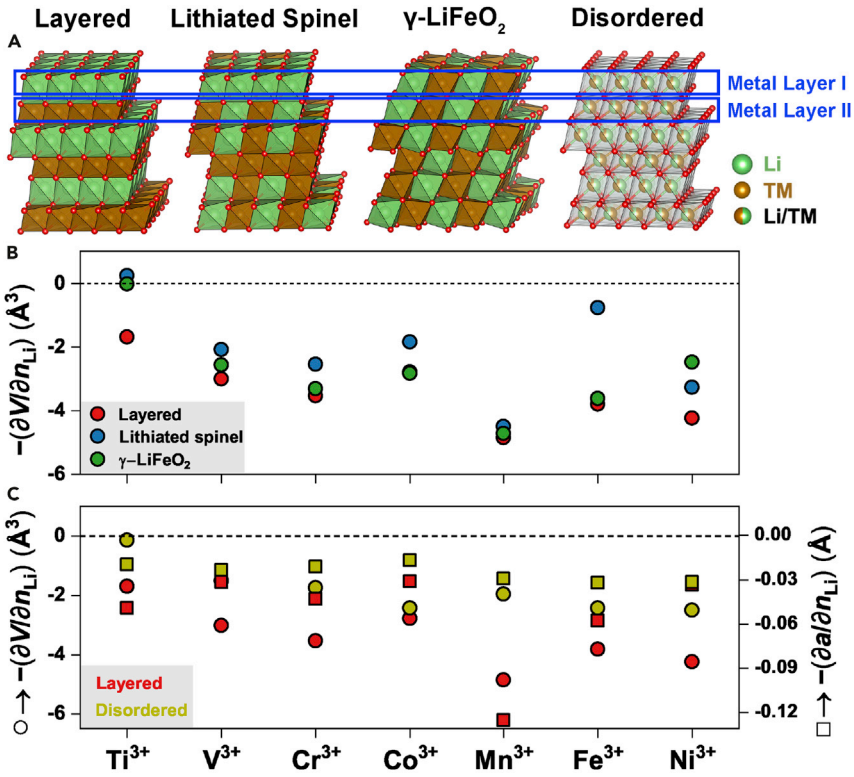

Figure 2. Effect of structure and cation ordering

(A) Structural model of, from left to right, layered, lithiated spinel, γ-$LiFeO_2$, and cation-disordered $LiMO_2$.

(B) Calculated partial molar extraction volume of Li in $LiMO_2$ in a layered (red circles), lithiated spinel (blue circles), and γ-$LiFeO_2$ structure (green circles).

(C) Partial molar extraction volume of Li (in circles) and partial molar lattice parameter upon delithiation (in squares) for layered (red) and cation-disordered structure (yellow).

average of the partial molar extraction volume of Li and the partial molar lattice parameters calculated from all the relaxed fully delithiated and lithiated structures. In Figure 2C, the left vertical axis corresponds to the partial molar extraction volume of Li (circles) and the right vertical axis corresponds to the negative partial molar lattice parameter (squares). For all chemistries, structures with cation mixing (in yellow) exhibit reduced volume reduction over layered structures (in red).

In lithiated spinel structures, Li can occupy both the octahedral (16c) and tetrahedral (8a) sites.[25] This gives us the ability to probe whether the partial molar volume of Li is different on the 8a and 16c site. In Figure 3A, we compare the volume change of two scenarios for delithiating a $Li_{0.5}MO_2$ composition with TM cations in the spinel-like 16d sites: In the first scenario (red points in Figure 3A), Li ions occupy the tetrahedral 8a sites. In the alternative scenario (green points in Figure 3A), Li ions occupy half of the octahedral 16c sites, with the distribution of Li and vacancies on 16c as the one that minimizes the electrostatic Ewald energy.[26] The partial molar extraction volume of Li, calculated by removing all the Li from the structure, is shown in Figure 3B. The structures with 8a occupancy have a greater magnitude of $-\overline{V}_{Li}$ compared with the structures with 16c occupancy for most of the chemistries, except for Ni^{3+} for which the $-\overline{V}_{Li}$ are very similar (−4.55 and −4.58 $Å^3$). For example, $Li_{0.5}TiO_2$ and $Li_{0.5}CoO_2$ have $-\overline{V}_{Li}$ of −1.92 and −2.91 $Å^3$ when Li occupies 8a sites but only −0.50 and −2.28 $Å^3$ when Li occupy 16c sites. We note that the average Li_{8a}–O bond length

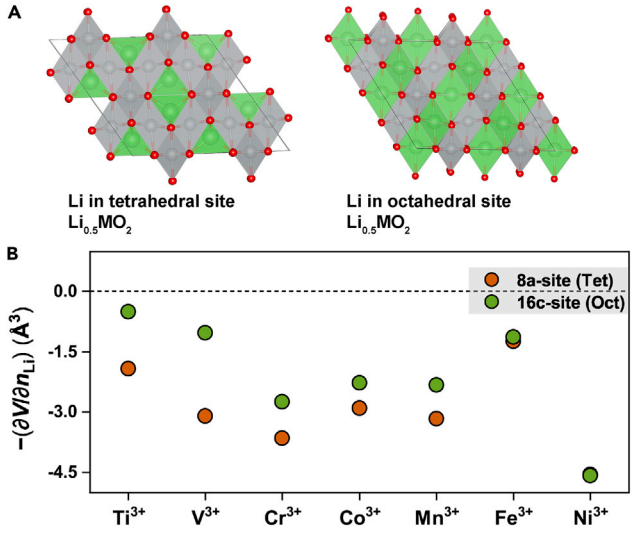

Figure 3. Effect of Li occupancy

(A) Tetrahedral (8a-site) versus octahedral (16c-site) insertion of Li in spinel-like host structure.

(B) Calculated partial molar extraction volume of Li from 8a (red) versus 16c (green) from $Li_{0.5}MO_2$ to MO_2.

(1.93 Å) is shorter than the average Li_{16c}–O bond length (2.11 Å), which is consistent with what one would expect from the Shannon radii.[27] Rather than the absolute volume, it is however the *change* in the size of the octahedron or tetrahedron that controls the partial molar Li volume. We will discuss this issue in a later section.

Detailed investigation of the Li^+–V^{3+}–Nb^{5+}–O^{2-}–F^- space

Some of the early TMs, such as Ti, V, and Cr, are good candidates to create low-strain cathode materials. Ti yields a low operating voltage, making it useful only for anode applications.[12,13] Due to its use of redox with t_{2g} states and reasonable voltage, we investigated the LVNOF DRX system in more detail. V^{3+}-based DRX materials are a promising class, given their high operating voltage, large reversible capacity, and synthetic accessibility.[16,17] The Nb^{5+} serves as a high-valence, redox-inert charge compensator that allows for more Li excess and has been used in multiple DRX cathodes.[17,28,29] In addition, substitution of some O^{2-} by F^- ensures a reasonable amount of electron capacity as well as improved cyclability.[30,31]

Using the cluster-expansion model and Monte Carlo (MC) simulations, we evaluate the volume change associated with delithiation of LVNOF compositions within the ternary phase diagram with $LiVO_2$, Li_3NbO_4, and LiF as the three endpoints, as shown in Figure 4A. Since LiF solubility is generally limited in DRX systems to 7%–10%,[32] we only consider compositions in which the F content is lower than 0.4 per formula unit, which is represented by the pink line in Figure 4A. Furthermore, we only consider compositions with a Li content between 1.0 and 1.4 per formula unit to ensure enough TM redox capability, as indicated by the blue line. The shaded region bounded by the constraints on F content (pink) and extractable Li (blue) thus indicates the region of interest for potential zs cathodes. The contour lines in this phase diagram show the compositions that share the same LiF solubility temperature based on cluster-expansion MC simulation. At nineteen compositions within these bounds, indicated by the black diamonds in Figures 4B and 4C, 10 disordered structures were sampled from a cluster-expansion MC simulation at elevated temperature. The specific compositions are given in Figure S2.

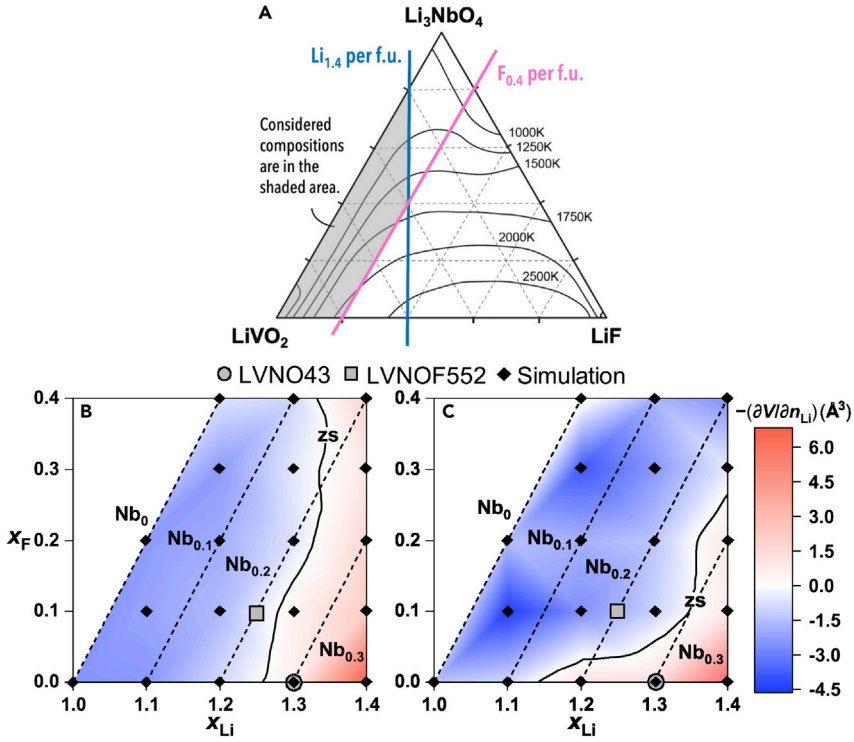

Figure 4. Calculated volume change of delithiation in LVNOF system

(A) Calculated phase diagram (per atom basis) highlighting the composition space that is expected to be synthetic accessible through solid-state synthesis and has reasonable electron capacity. Calculated and interpolated partial molar extraction volume of Li when delithiated by (B) all $V^{3+\rightarrow 5+}$ capacity and (C) 0.2 Li/anion. All simulated LVNOF compositions are denoted by the black diamonds. The locations of the two experimental compositions synthesized in this work are denoted by the closed circle and square. The "zs" denotes the zero-strain contour. See also Figure S2 for the exact simulated compositions.

For each MC-sampled lithiated structure, we evaluated the volume change to two different levels of delithiation: (1) removing a fixed number of 0.2 Li/anion to evaluate the volume change at low levels of charge and (2) removing the number of Li that can be fully charge-compensated by the V^{3+}/V^{5+} redox without triggering oxygen redox, which can complicate the volume change trend in materials. Figures 4B and 4C show the partial molar extraction volumes of Li interpolated between the investigated compositions as a color map. The dashed lines represent constant Nb content. A band of zs compositions near the solid line labeled as "zs" is found for Nb content between 0.2 and 0.3 and Li excess of 0.25–0.3. Two major trends can be recognized in the map. First, as the Nb content increases, the partial molar extraction volume of Li generally becomes less negative. Second, the dependence of partial molar extraction volume of Li on the fluorination level is weak in the LVNOF system.

To experimentally confirm our predictions for the partial molar extraction volume of Li, we synthesized two compounds in the vicinity of the predicted zs composition contour (Figures 4B and 4C, circle and square symbols), LVNO43 and LVNOF552, via a solid-state synthesis method. Details of the synthesis are provided in the experimental procedures section. The X-ray diffraction (XRD) patterns of both materials are presented in Figures S5A and S5C and can be indexed to a disordered rocksalt phase (Fm-3m) without any apparent impurity peaks. Figures S5B and S5D show the

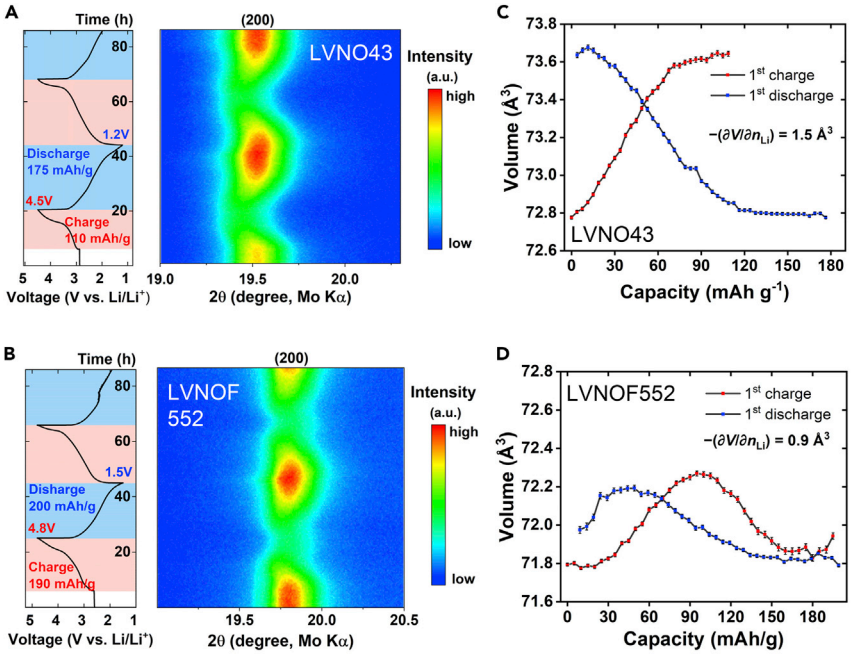

Figure 5. Structural change of LVNO43 and LVNOF552 during cycling

In situ XRD and corresponding electrochemical profile for the first 2 cycles under 10 mAg^{-1} of (A) $Li_{1.3}V_{0.4}Nb_{0.3}O_2$ (LVNO43) and (B) $Li_{1.25}V_{0.55}Nb_{0.2}O_{1.9}F_{0.1}$ (LVNOF552); variations of unit-cell volume of (C) $Li_{1.3}V_{0.4}Nb_{0.3}O_2$ and (D) $Li_{1.25}V_{0.55}Nb_{0.2}O_{1.9}F_{0.1}$.

See also Figure S5.

electrochemical cycling of LVNO43 and LVNOF552, respectively. A reversible discharge capacity higher than 275 mAh/g (corresponding to an extractable amount of 0.46 Li/anion or 0.92 Li per formula unit) is obtained in both cathodes at a current density of 10 mA/g, similar to previously reported results.[33] The change of lattice parameters of LVNO43 and LVNOF552 with delithiation was evaluated using *in situ* XRD and is presented in Figures 5A and 5B. Figures 5C and 5D also give the refined volume of the two cathode materials at each SOC. It is noted that Equation 1 was not used for approximating the volume change of delithiation for LVNO43 and LVNOF552 because the volume does not increase (decrease) monotonically during discharge (charge), especially for LVNOF552. Instead, the partial molar extraction volume of Li was obtained by normalizing the difference between the maximum and minimum unit-cell volume by extracted Li content. This approach can account for the upper limit of the overall volume change throughout the entire operation voltage range and may yield greater magnitude of partial molar extraction volume of Li than that computed from Equation 1. As shown in Figure 5C, LVNO43 exhibits a maximum 1.2% volume change over a capacity of ~175 mAh/g, corresponding to a $-\overline{V}_{Li}$ of 1.5 $Å^3$, in line with our theoretical prediction of $-\overline{V}_{Li}$ equal to 1.3 $Å^3$. The fluorinated compound (i.e., LVNOF552) exhibits a lower volume change of 0.7% over a capacity of ~200 mAh/g, corresponding to a $-\overline{V}_{Li}$ of 0.9 $Å^3$. Our calculation predicts a similarly small $-\overline{V}_{Li}$ of −0.5 $Å^3$ per stoichiometric Li.

Effect of metal migration

In some cathode materials, TMs may migrate back and forth between tetrahedral and octahedral sites as their oxidation state changes. Migration to a tetrahedral site is particularly likely for V and Cr containing materials when they are fully oxidized at the top of charge[16,17,34] and potentially for some Fe-containing oxides.[35,36] To

Please cite this article in press as: Zhao et al., Design principles for zero-strain Li-ion cathodes, Joule (2022), https://doi.org/10.1016/j.joule.2022.05.018

Table 1. Fitted 1st-order coefficient of partial molar extraction volume of Li in two cases of delithiation

	Remove 0.2 Li/anion		Using $V^{3+ \rightarrow 5+}$ capacity	
Variable	Coeff. (Å^3)	R^2-score (RMSE [Å^3])	Coeff. (Å^3)	R^2-score (RMSE [Å^3])
Li_{tet}	19.6	0.734 (1.36 Å^3)	14.5	0.729 (1.34 Å^3)
V_{tet}	11.1		18.2	
Nb	16.4		16.0	
F	−1.67		2.10	
Intercept	−2.92		−2.99	

See also Figures S3 and S4, Table S2, and Note S1.

establish a quantitative model for predicting volume change in LVNOF DRX and to more comprehensively understand the impact of any changing site occupancies during delithiation on the volume change, we linear regressed the partial molar extraction volume of Li against the site occupancies,[37,38] which are defined as the concentration of site-distinguished species with respect to the total number of anions in the simulated structure. Because the site occupancies of certain species are correlated, e.g., the occupancy of O and F on the anion site sums to one, we fitted with various sets of features and chose the set that minimizes correlation among the site variables while maintaining reasonable prediction power (see also Figures S3 and S4, Table S2, and Note S1). The features used for the fitting of the partial molar extraction volume of Li include the concentration of tetrahedral Li and V, octahedral Nb, and F in the delithiated structures. The fitting coefficients for both the limited delithiation and full redox-capable delithiation are shown in Table 1. The intercept term is interpreted as the average partial molar extraction volume of Li of disordered rocksalt $LiVO_2$ (all four features equal 0). From Table 1, for both cases of delithiation, we observe that the tetrahedral Li and V and the octahedral Nb have positive coefficients, indicating that more of their presence in the delithiated structure makes the partial molar extraction volume of Li less negative. The coefficients of F, however, are small, indicating a much weaker dependence of the partial molar extraction volume of Li on F, consistent with the trend observed in Figures 4B and 4C.

DISCUSSION

In this work, we have deconvoluted the factors that control the volume change when cathode oxides are delithiated, thereby providing insight and a potential pathway toward cathode materials with low strain. Although achieving a small dimensional variation during charge and discharge is important for all intercalation-based energy storage, it may be particularly critical for SSBs, where the lack of compliance of the solid electrolyte can lead to interface decohesion between the cathode and electrolyte.[7,39]

We find that in most cases, Li removal from the oxides leads to a volume reduction, consistent with the expectations that the Li^+ cation has a positive partial molar volume and that oxidation reduces the size of the TM. However, the partial molar volume of Li in cathode materials (2–5 Å^3 in layered oxides) is almost an order of magnitude smaller than the volume of Li metal (21.6 Å^3/atom),[40] highlighting the fundamentally different energetics in the oxide and metal. We find that the orbital symmetry of the electron that is removed by oxidation (t_{2g} versus e_g) is an important factor in setting the volume change, with a TM with an e_g electron typically having 2–4 Å^3/Li larger volume contraction compared with the oxidation of a t_{2g} state. This is consistent with our understanding of the nature of these electron states: although the e_g states are the antibonding counterpart of the (bonding) oxygen-rich states, the t_{2g} states can be considered mostly non-bonding in character[41] as they have

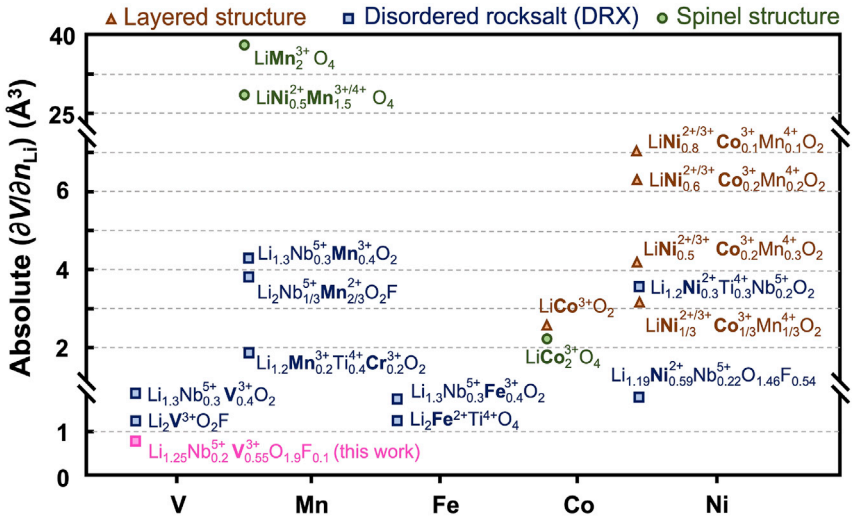

Figure 6. Summary of absolute partial molar volume of Li of selected reported cathodes

The valence states of the TM ions in the fully lithiated compounds are decorated in the formula, and the TM redox centers are highlighted in bold font. Note that the spinel structures in this plot have a cation:anion ratio of 3:4, which is different from the lithiated spinel structures used in the DFT calculation with a cation:anion ratio of 1:1.

no net σ-overlap with the *p* orbital of oxygen. Hence, removing an electron from the t_{2g} states has a limited effect on the TM–O bond length. In contrast, removing an antibonding e_g electron from the TM upon reduces the TM–O bond length. As a result, the TM–O bond shortens more severely for the e_g-redox- than for the t_{2g}-redox-based system.[42,43] For Mn^{3+}- and Fe^{3+}-containing compounds, the volume change associated with the removal of Li is also affected by the JT distortion associated with high-spin Mn^{3+} and Fe^{4+}, as illustrated in Figures S1B and S1C. The anharmonic part of a JT distortion in the typical positive Q_3 mode (two elongated and four shortened bonds) leads to a volume expansion.[41] This is particularly true for ions with large JT distortions such as Mn^{3+} and Fe^{4+} and less so for Ni^{3+} for which the JT distortion is smaller and less anharmonic. Hence, the volume reduction from $LiMnO_2$ to MnO_2 is particularly large as oxidation compounds the removal of an e_g electron with the loss of the JT activity. In $LiFeO_2$, the JT ion Fe^{4+} is instead created upon charging, thereby mitigating the volume reduction from the removal of an e_g electron, leading to an overall smaller volume change than expected as can be observed in Figure 1. With this perspective, $Fe^{3+/4+}$ oxidation would result in a particularly attractive combination of low strain and reasonable voltage, making it unfortunate that few Fe-containing close-packed oxides lead to functioning cathode materials,[44–46] possibly due to the migration of Fe^{3+} whenever Li vacancies are created.[47]

Our computational findings are well corroborated by experimental data. In Figure 6, we show the absolute partial molar volumes of Li obtained from the lattice-parameter changes as measured in the literature with XRD.[1,14,28,29,34,48–55] The data are sorted by active TM (x axis) and by structure (shape of symbol and color). The experimental data support that Mn-redox-based compounds generally exhibit larger volume change than compounds with Fe or with TM ions that have an t_{2g} electrons removed upon oxidation. Figure 6 also confirms the low volume change of cathodes with V-based redox since oxidation only removes t_{2g} electrons.

Our analysis of the structural effect on the volume of delithiation (Figure 2B) shows variations of 1–2 $Å^3$/Li among the different cation arrangements. Among the

Please cite this article in press as: Zhao et al., Design principles for zero-strain Li-ion cathodes, Joule (2022), https://doi.org/10.1016/j.joule.2022.05.018

ordered compounds, the cubic lithiated spinel generally undergoes the smallest volume change, whereas the layered structure tends to have the largest volume change. Disordered rocksalts have similar or slightly lower volume change than the lithiated spinels, hinting at the fact that the isotropic character of their crystal structure is important to achieve low volume change. Our computational findings on the role of structure are also supported by the experimental data in Figure 6. In the Ni-redox based compounds provided in Figure 6, layered NCM materials, except for $LiNi_{1/3}Co_{1/3}Mn_{1/3}O_2$, have a larger magnitude of Li partial molar volume than the disordered rocksalt structures ($Li_{1.2}Ni_{0.3}Ti_{0.3}Nb_{0.2}O_2$ and $Li_{1.19}Ni_{0.59}Nb_{0.22}O_{1.46}F_{0.54}$). Even for compounds undergoing oxidation of the Mn^{3+} ion, which displays one of the largest intrinsic volume changes, fairly low volume changes can be obtained: for example, the recently reported $Li_{1.2}Mn_{0.2}Ti_{0.4}Cr_{0.2}O_2$ DRX, in which both Mn^{3+} and Cr^{3+} are redox active, but in which Cr^{6+} migrates to a tetrahedral site at top of charge, exhibits an absolute partial molar volume of Li of only 1.96 $Å^3$/Li evaluated at a capacity of 257 mAh/g.[34] Hence, retaining high symmetry, either by selection of the cation order to be isotropic or by cation disordering, is a powerful handle to reduce volume change.

In addition to the TM redox center and cation ordering, the anion coordination of Li also affects its partial molar volume. The results in Figure 3B demonstrate that the partial molar volume of tetrahedral Li is larger than that of octahedral Li. Although this may seem inconsistent with the bond lengths given earlier, it is the change in this polyhedral volume upon Li insertion or extraction that is relevant. We find that upon delithiation, the size of the tetrahedron changes comparatively more than the size of the Li octahedron, which results in a smaller volume change for insertion or removal of octahedral Li. The greater volume contribution of the tetrahedral Li presents a real advantage for DRX materials as they contain some vacant tetrahedral sites that are only face-sharing with octahedral Li.[15] These 0-TM tetrahedral sites can become occupied once enough Li is removed,[56] adding a positive volume contribution upon charge. The higher partial molar volume of Li_{tet} also explains the observation by Lee et al. that the lithiated spinel $Li_2(Co_{1-x}Al_x)_2O_4$ manifests very little change in its volume (0.02%) when half of the Li ions are removed to form $Li(Co_{1-x}Al_x)_2O_4$.[57] When Li is removed from this lithiated spinel, the remaining Li ions migrate from the 16c to 8a sites as is well documented for other spinels such as LTO and $Li_2Mn_2O_4$.[58,59] This migration of the remaining Li from 16c to 8a sites compensates for the volume reduction from the oxidation of Co^{3+} to Co^{4+} and removal of half the Li ions upon charging. The formation of tetrahedral Li upon charging has also been documented in layered materials that have Li excess in the TM layer.[60,61]

Although our findings on the role of the TM cation, the structure, and the Li coordination should be general, we have studied in more detail in this paper the role of other factors such as F substitution of O and the addition of inactive metals in setting the volume change of disordered rocksalt compounds. In LVNOF compounds, the redox-inactive charge compensator Nb^{5+} ions remain octahedrally coordinated with the anions upon charge. We have also found that the average Nb–O bond length undergoes a negligible change of 0.01 Å (~0.5%) upon delithiation, indicating that the NbO_6 unit serves as a rigid pillar that limits the contraction of the unit-cell volume upon delithiation, consistent with the positive regressed coefficients for Nb in Table 1. Hence, redox-inactive metals may limit the volume reduction associated with Li removal by constraining how much TM and octahedra can change volume. In contrast, we find that substitution of O by F does little to modify the Li partial molar volume.

Please cite this article in press as: Zhao et al., Design principles for zero-strain Li-ion cathodes, Joule (2022), https://doi.org/10.1016/j.joule.2022.05.018

Furthermore, it is crucial to recognize that the oxidation of redox-active TM upon charge can be accompanied by site migration,[17,34,36,62] which also affects the volume change of DRX compounds. In LVNOF, V can only migrate from a Li_3V tetrahedral configuration of octahedral sites (a vacant tetrahedral site with one V and three Li first nearest neighbors)[17] when the three oct-Li ions are removed so that no face-sharing Li neighbors remain for the tetrahedral V. It can be inferred from our linear fitting in Table 1 that tetrahedral V leads to a reduced volume contraction in the V-containing DRX compounds. The increasing tetrahedral occupancy of TM ions can further minimize volume strain in disordered rocksalt compounds, especially with highly oxidized metals such as V^{5+}, Cr^{6+} or for d^5 ions such as Mn^{2+} and Fe^{3+}, which favors an oct-to-tet migration.[17,34,63] This effect of cation migration upon oxidation on the partial molar extraction volume of Li aligns well with a recent study by Huang et al., which notes that the introduction of reversible oct-tet migration of Cr as one of the redox centers in the Li^+–Mn^{3+}–Ti^{4+}–Cr^{3+}–O^{2-} DRX system not only improves the rate performance but also results in smaller volume change normalized by capacity, compared with the Cr-free Li^+–Mn^{3+}–Ti^{4+}–O^{2-} DRX system.[34]

Our findings show that the cation-disordered rocksalt (DRX) and spinel structure are good crystal structures from which to design low-strain cathode materials. DRX cathodes have the additional advantage that they can incorporate some of the other design handles that we have discussed in this paper, including inactive components, migration of Li from octahedral to tetrahedral sites upon charge, and reversible migration of oxidized TMs. In this paper, we have demonstrated very low volume change in LVNO43 and LVNOF552, making them interesting candidates for solid-state battery cathodes.

Although cation disordering cannot be used to lower the volume change of layered cathodes as it reduces the mobility,[64] one can still apply the other design criteria identified in this paper to optimize dimensional change upon delithiation. Experimentally, de Biasi et al. demonstrated that increasing the Co content in NCM systems can effectively reduce the volumetric strain across a wide range of charging voltages from 3.6 to 4.6 V.[14] This observation aligns well with our theoretical arguments, as the high-spin Co, with only t_{2g} electrons involved in the oxidation, tends to induce much smaller volume changes upon delithiation than the $Ni^{2+/3+}/Ni^{4+}$ redox. According to our findings, it should also be possible to introduce stabilizing cations into the TM layers to reduce the strain. For example, Mn^{4+} has been experimentally used as a structural stabilizer in the layered $LiNiO_2$ (LNO) system, in which Ni^{2+}/Ni^{4+} is the only redox couple.[65–67] Our preliminary calculation on the $LiNi_{1-x}Mn_xO_2$ ($0 < x < 0.5$) systems suggests that the redox-inert Mn^{4+} can ameliorate the in-plane contraction upon delithiation and reduce the volume change when all the Li ions are extracted (see Figure S6 and supplemental information). This result agrees with a study by Yang et al., which shows that the change of both a- and c-parameters upon charge is smaller for $LiNi_{0.5}Mn_{0.5}O_2$ than for $LiNiO_2$ for comparable amounts of Li extraction.[68] In addition, it may also be possible to reduce the volume change of lithiated spinel (cation:anion = 1:1) materials. Although isotropic cation ordering and tetrahedral Li occupancy help to reduce the volume change of delithiation, the long-range ordering of JT-active cations in the spinel structure can cause a large volume change by inducing a collective distortion, as exemplified by $LiMn_2O_4$ in Figure 6. Therefore, it is also possible to further suppress the volume change in spinel systems by introducing cation disorder. Enough of such cation disorder should disrupt the collective JT distortion so that the JT-active ions distort in different modes instead of only the Q_3 mode.[41,69]

Please cite this article in press as: Zhao et al., Design principles for zero-strain Li-ion cathodes, Joule (2022), https://doi.org/10.1016/j.joule.2022.05.018

Conclusions

In this study, we established general principles for the design of low-strain cathodes based on materials with an FCC anion framework. We showed that transition-metal redox centers with non-bonding electronic configurations, isotropic structures, cation disordering, inactive elements, and octahedral-to-tetrahedral migration of Li upon charging reduce the volume change associated with delithiation. These principles were applied to two compositions in the LVNOF DRX system that were experimentally observed to be quasi-zs, validating the general design principles. Our guidelines provide new insights into minimizing the strain of electrochemical cycling for cathode candidates based on not only the DRX structure but also for layered and spinel frameworks.

EXPERIMENTAL PROCEDURES

Resource availability

Lead contact

Further information and requests for resources and materials should be directed to and will be fulfilled by the lead contact, Gerbrand Ceder (gceder@berkeley.edu).

Materials availability

Materials generated in this study will be made available on request.

Data and code availability

Experimental or computational data and codes are available on request.

Synthesis

LVNO43 was synthesized using a solid-state sintering method. Li_2CO_3 (with 5% excess), V_2O_3, and Nb_2O_5 in a stoichiometric ratio were mixed and pre-heated in Ar at 650°C and held for 1 h, followed by sintering at 950°C for 7 h. The resulting sample was then cooled to room temperature and ball milled using a Retsch PM 400 planetary ball mill at 180 rpm for 2 h to attain a uniform particle size. $Li_{1.25}V_{0.55}Nb_{0.2}O_{1.9}F_{0.1}$ was synthesized using a similar solid-state sintering method. Li_2CO_3 (with 5% excess), V_2O_3, Nb_2O_5, and LiF in a stoichiometric ratio were mixed and pre-heated in Ar at 650°C and held for 1 h, followed by sintering at 950°C for 7 h. The resulting sample was then ambient air quenched (without being exposed to air). Different cooling methods in the synthesis of $Li_{1.25}V_{0.55}Nb_{0.2}O_{1.9}F_{0.1}$ are compared in Figure S7. The sample was then transferred to an Ar-filled glovebox and ball milled using a Retsch PM 400 planetary ball mill at 180 rpm for 2 h to attain a uniform particle size.

Electrochemistry

All the cathode films were composed of the active materials, Super C65 (Timcal), and polytetrafluoroethylene (PTFE, DuPont, Teflon 8A) in a weight ratio of 7:2:1. To make the cathode films, the hand-ground cathode materials and Super C65 in the above ratio were mixed and shaker-milled for 90 min in an Ar-filled glovebox using a SPEX 800M mixer, after which PTFE was added and manually mixed for 30 min. The composite was then rolled into thin films inside a glovebox. A commercial electrolyte of 1 M $LiPF_6$ in ethylene carbonate and dimethyl carbonate solution (1:1 volume ratio) was used. A glass microfiber filter (Whatman) was used as the separator. FMC Li-metal foil was used as the anode. Coin cells were assembled in an Ar-filled glovebox and tested on an Arbin battery testing instrument at room temperature at a galvanostatic charge/discharge rate of 10 mA g^{-1}.

Characterization

The structures of the obtained materials were analyzed using XRD (Rigaku Miniflex 600) with Cu Kα radiation. The particle morphology was verified using field-emission scanning electron microscopy (FE-SEM, Zeiss Gemini Ultra-55). Transmission electron microscopy (TEM) samples were prepared by drop casting the solution onto a standard 400 copper-mesh TEM grid with lacey carbon support in an Ar-filled glovebox. The scanning transmission electron microscopy with energy-dispersive X-ray spectroscopy (STEM-EDX) characterizations were performed using JEM-2010F and Titan X microscopes. *In situ* electrochemical tests were performed using a customized cell with a beryllium window to allow X-ray penetration. The XRD measurements were performed on a Bruker D8 diffractometer using Bragg-Brentano geometry with Mo Kα radiation. Each scan was performed for 1 h while the cell was cycled at C/20 for two full cycles. The Rietveld refinement was performed using TOPAS software 6.0.[70]

Computational methods

A complete model for the configurational thermodynamics of LVNOF must account for the Li and TM distributions on the cation sublattice as well as the O/F arrangement on the anion sublattice. Such a system with coupled disorder on multiple sublattices can be well studied using the coupled cluster-expansion approach.[71] The cluster-expansion model has been demonstrated to be an effective method to capture long-range order in intercalation cathodes[72,73] as well as short-range order in DRX systems.[30,32,56,74] In a cluster expansion, the configurational-energy dependence is captured by an expansion into different cluster functions, which can be formulated as[37,75]

$$E = \sum_{i,sp1} J_i^{sp1} \sigma_i^{sp1} + \sum_{i,j,sp1,sp2} J_{ij}^{sp1sp2} \sigma_i^{sp1} \sigma_j^{sp2} + \sum_{i,j,k,sp1,sp2,sp3} J_{ijk}^{sp1sp2sp3} \sigma_i^{sp1} \sigma_j^{sp2} \sigma_k^{sp3} \ldots \ldots \quad \text{(Equation 2)}$$

Here, σ_i^{sp} corresponds to the occupancy of a certain site(s) with a certain species *sp*, and *J* refers to the effective cluster interactions (ECIs). In our system of LVNOF, pair interactions up to 7.1 Å, triplet interactions up to 4.0 Å, and quadruplet interactions up to 4.0 Å based on a rocksalt lattice with a cubic lattice parameter a = 3.0 Å were included in the cluster-expansion formalism. All interactions were taken with respect to a baseline electrostatic energy defined using the formal charges of the ionic species and a dielectric constant which is fitted together with the ECIs. The ECIs were fitted to DFT energies of sampled structures using a L_1-regularized least-squares regression approach,[76] with the regularization parameters selected to minimize the cross-validation score.[76] The cluster expansion was fitted with a root-mean-squared error of less than 7 meV/atom. The minimized cross-validation errors were converged to less than 10 meV/atom as well.

With the constructed cluster expansion, we performed finite-temperature configuration sampling with canonical MC using the Metropolis-Hastings algorithm.[77] For each sampled composition and temperature, the equilibration consisted of 8,000,000 MC steps, and the production consisted of 8,000,000 MC steps. A total of 1,000 MC structures were sampled during the production run; from this, we selected 10 structures on which to perform DFT calculations to obtain the volume and locally relaxed atomic positions. For the compounds with 0.0, 0.2, and 0.4 F per formula unit, the MC was performed using a 2 × 2 × 5 supercell. For F contents of 0.1 and 0.3, a 2 × 4 × 5 supercell was used to ensure an integer number of all the atoms in the cell.

All the energetics, structures, and oxidation states of the studied cathode materials were obtained from first-principles computation using the projector-augmented wave (PAW) method[78] implemented in the Vienna *ab initio* simulation package

(VASP).[79] The SCAN+rVV10 functional was used to consider intermediate-to-long-range van der Waals interactions[80,81] to more accurately describe structural changes associated with (de)lithiation of the FCC polymorphs of the cathode materials. For all our calculations, a plane-wave basis set with an energy cut-off of 520 eV and a reciprocal space discretization of 25 k-points/Å were adopted. The total energies were converged to 10^{-6} eV for the electronic loops and interatomic forces were converged to 0.02 eV $Å^{-1}$ for ionic loops.

For layered $LiMO_2$, the partial molar lattice parameter was taken as the change of c-parameter (out-of-layer direction) upon delithiation normalized by the number of extracted Li to account for the anisotropic strain. However, for the cubic disordered rocksalt $LiMO_2$, an isotropic volume change was assumed and the partial molar lattice parameter was approximated from the average change of all three lattice parameters upon delithiation normalized by the number of removed Li.

The regression model for fitting the partial molar extraction volume of Li uses L_1-regularization with an objection function of

$$\underset{\mathbf{v}}{\operatorname{argmin}}\left(\frac{1}{2}\|\mathbf{Xv}-\mathbf{y}\|_2^2+\lambda\|\mathbf{v}\|_1\right),\quad s.t.\ \mathbf{y}=\mathbf{Xv}, \qquad \text{(Equation 3)}$$

where $\mathbf{X}$ is the site occupancy matrix, $\mathbf{y}$ contains all the partial molar extraction volumes of Li, λ is a coefficient that weighs the L_1-norm penalty and $\mathbf{v}$ contains the fitted coefficients of partial molar extraction volumes of Li. The site occupancy is defined as the concentration of each species normalized by the total number of anions in the delithiated structure, including Li_{tet}, Li_{oct}, V_{tet}, V_{oct}, Nb_{oct}, O, and F. Since the occupancies are constrained by site and charge conservations, the 7 degrees of freedom (DOFs) reduce to 4 DOFs. The detailed process for feature selection for the regression model is discussed in the supplemental experimental procedure. To minimize the correlation among site variables Li_{tet}, V_{tet}, Nb_{oct} and F were selected as the feature set used in the linear regression.

SUPPLEMENTAL INFORMATION

Supplemental information can be found online at https://doi.org/10.1016/j.joule.2022.05.018.

ACKNOWLEDGMENTS

Work at the Molecular Foundry was supported by the Office of Science and Office of Basic Energy Sciences of the US DOE under contract no. DE-AC02-05CH11231. The computational analysis was performed using computational resources sponsored by the DOE's Office of Energy Efficiency and Renewable Energy and located at the National Renewable Energy Laboratory. Computational resources were also provided by the Extreme Science and Engineering Discovery Environment (XSEDE), supported by National Science Foundation grant number ACI1053575, and the National Energy Research Scientific Computing Center (NERSC), a DOE Office of Science User Facility supported by the Office of Science and the U.S. Department of Energy under contract no. DE-AC02-05CH11231. This research also used the Lawrencium computational cluster resource provided by the IT Division at Lawrence Berkeley National Laboratory (supported by the Director, Office of Science, Office of Basic Energy Sciences of the U.S. Department of Energy under contract no. DE-AC02-05CH11231). We also acknowledge the support by the Assistant Secretary for Energy Efficiency and Renewable Energy, Vehicle Technologies Office, under the Applied Battery Materials Program, of the U.S. Department of Energy under

contract no. DE-AC02-05CH11231. We thank Dr. Daniil Kitchaev, Dr. Yaqian Zhang, and Mr. Kelvin Ye for their valuable input on this study.

AUTHOR CONTRIBUTIONS

B.O. and G.C. conceived the idea and planned the project. G.C. supervised all aspects of the research. X.Z. and B.O. performed the *ab initio* calculations and analyzed the results. With the help of Z.L, Z.C., T.C., and Y.T. synthesized, characterized, and electrochemically tested the proposed materials. The manuscript was written by X.Z. and G.C. and was revised by other co-authors. All the authors contributed to the discussions.

DECLARATION OF INTERESTS

G.C. is a member of the journal's advisory board. The authors declare no other competing interests.

Received: February 14, 2022
Revised: April 28, 2022
Accepted: May 26, 2022
Published: June 17, 2022

REFERENCES

1. Strauss, F., de Biasi, L., Kim, A.-Y., Hertle, J., Schweidler, S., Janek, J., Hartmann, P., and Brezesinski, T. (2020). Rational design of quasi-zero-strain NCM cathode materials for minimizing volume change effects in all-solid-state batteries. ACS Mater. Lett. *2*, 84–88.

2. Berg, H., and Thomas, J.O. (1999). Neutron diffraction study of electrochemically delithiated $LiMn_2O_4$ spinel. Solid State Ion *126*, 227–234.

3. Padhi, A.K., Nanjundaswamy, K.S., and Goodenough, J.B. (1997). Phospho-olivines as positive-electrode materials for rechargeable lithium batteries. J. Electrochem. Soc. *144*, 1188–1194.

4. Yamada, A., Koizumi, H., Sonoyama, N., and Kanno, R. (2005). Phase change in Li_xFePO_4. Electrochem. Solid State Lett. *8*, A409.

5. Kondrakov, A.O., Schmidt, A., Xu, J., Geßwein, H., Mönig, R., Hartmann, P., Sommer, H., Brezesinski, T., and Janek, J. (2017). Anisotropic lattice strain and mechanical degradation of high- and low-nickel NCM cathode materials for Li-ion batteries. J. Phys. Chem. C *121*, 3286–3294.

6. Samsung US Newsroom. (2017). Samsung Announces Cause of Galaxy Note7 Incidents in Press Conference. https://news.samsung.com/us/Samsung-Electronics-Announces-Cause-of-Galaxy-Note7-Incidents-in-Press-Conference.

7. Shi, T., Zhang, Y.-Q., Tu, Q., Wang, Y., Scott, M.C., and Ceder, G. (2020). Characterization of mechanical degradation in an all-solid-state battery cathode. J. Mater. Chem. A *8*, 17399–17404.

8. Koerver, R., Aygün, I., Leichtweiß, T., Dietrich, C., Zhang, W., Binder, J.O., Hartmann, P., Zeier, W.G., and Janek, J. (2017). Capacity fade in solid-state batteries: interphase formation and chemomechanical processes in nickel-rich layered oxide cathodes and lithium thiophosphate solid electrolytes. Chem. Mater. *29*, 5574–5582.

9. Koerver, R., Zhang, W., Biasi, L. de, Schweidler, S., Kondrakov, A.O., Kolling, S., Brezesinski, T., Hartmann, P., Zeier, W.G., and Janek, J. (2018). Chemo-mechanical expansion of lithium electrode materials – on the route to mechanically optimized all-solid-state batteries. Energy Environ. Sci. *11*, 2142–2158.

10. Fan, X., Hu, G., Zhang, B., Ou, X., Zhang, J., Zhao, W., Jia, H., Zou, L., Li, P., and Yang, Y. (2020). Crack-free single-crystalline Ni-rich layered NCM cathode enable superior cycling performance of lithium-ion batteries. Nano Energy *70*, 104450.

11. Ruess, R., Schweidler, S., Hemmelmann, H., Conforto, G., Bielefeld, A., Weber, D.A., Sann, J., Elm, M.T., and Janek, J. (2020). Influence of NCM particle cracking on kinetics of lithium-ion batteries with liquid or solid electrolyte. J. Electrochem. Soc. *167*, 100532.

12. Zaghib, K., Armand, M., and Gauthier, M. (1998). Electrochemistry of anodes in solid-state Li-ion polymer batteries. J. Electrochem. Soc. *145*, 3135–3140.

13. Ohzuku, T., Ueda, A., and Yamamoto, N. (1995). Zero-strain insertion material of Li $[Li_{1/3}Ti_{5/3}]O_4$ for rechargeable lithium cells. J. Electrochem. Soc. *142*, 1431–1435.

14. de Biasi, L., Kondrakov, A.O., Geßwein, H., Brezesinski, T., Hartmann, P., and Janek, J. (2017). Between Scylla and Charybdis: balancing Among structural stability and energy density of layered NCM cathode materials for advanced lithium-ion batteries. J. Phys. Chem. C *121*, 26163–26171.

15. Lee, J., Urban, A., Li, X., Su, D., Hautier, G., and Ceder, G. (2014). Unlocking the potential of cation-disordered oxides for rechargeable lithium batteries. Science *343*, 519–522.

16. Yabuuchi, N., Nakayama, M., Takeuchi, M., Komaba, S., Hashimoto, Y., Mukai, T., Shiiba, H., Sato, K., Kobayashi, Y., Nakao, A., et al. (2016). Origin of stabilization and destabilization in solid-state redox reaction of oxide ions for lithium-ion batteries. Nat. Commun. *7*, 13814.

17. Nakajima, M., and Yabuuchi, N. (2017). Lithium-excess cation-disordered rocksalt-type oxide with nanoscale phase segregation: $Li_{1.25}Nb_{0.25}V_{0.5}O_2$. Chem. Mater. *29*, 6927–6935.

18. Peng, H., Yang, Z.-H., Perdew, J.P., and Sun, J. (2016). Versatile van der Waals Density Functional Based on a Meta-Generalized Gradient Approximation. Phys. Rev. X *6*, 041005.

19. Yang, J.H., Kitchaev, D.A., and Ceder, G. (2019). Rationalizing accurate structure prediction in the meta-GGA SCAN functional. Phys. Rev. B *100*, 035132.

20. Chakraborty, A., Dixit, M., Aurbach, D., and Major, D.T. (2018). Predicting accurate cathode properties of layered oxide materials using the SCAN meta-GGA density functional. npj Comput. Mater. *4*, 1–9.

21. Urban, A., Abdellahi, A., Dacek, S., Artrith, N., and Ceder, G. (2017). Electronic-structure origin of cation disorder in transition-metal oxides. Phys. Rev. Lett. *119*, 176402.

22. Gispert, J.R. (2008). Coordination Chemistry (Wiley-VCH).

23. Rossen, E., Reimers, J.N., and Dahn, J.R. (1993). Synthesis and electrochemistry of spinel LT-$LiCoO_2$. Solid State Ion *62*, 53–60.

24. Urban, A., Matts, I., Abdellahi, A., and Ceder, G. (2016). Computational design and preparation of cation-disordered oxides for high-energy-density Li-ion batteries. Adv. Energy Mater. *6*, 1600488.

25. Wang, H., Jang, Y.-I., Huang, B., Sadoway, D.R., and Chiang, Y.-M. (1999). TEM study of electrochemical cycling-induced damage and disorder in $LiCoO_2$ cathodes for rechargeable lithium batteries. J. Electrochem. Soc. *146*, 473–480.

26. Toukmaji, A.Y., and Board, J.A. (1996). Ewald summation techniques in perspective: a survey. Comput. Phys. Commun. *95*, 73–92.

27. Shannon, R.D. (1976). Revised effective ionic radii and systematic studies of interatomic distances in halides and chalcogenides. Acta Cryst. A *32*, 751–767.

28. Yabuuchi, N., Takeuchi, M., Nakayama, M., Shiiba, H., Ogawa, M., Nakayama, K., Ohta, T., Endo, D., Ozaki, T., Inamasu, T., et al. (2015). High-capacity electrode materials for rechargeable lithium batteries: Li_3NbO_4-based system with cation-disordered rocksalt structure. Proc. Natl. Acad. Sci. USA *112*, 7650–7655.

29. Wang, R., Li, X., Liu, L., Lee, J., Seo, D.-H., Bo, S.-H., Urban, A., and Ceder, G. (2015). A disordered rock-salt Li-excess cathode material with high capacity and substantial oxygen redox activity: $Li_{1.25}Nb_{0.25}Mn_{0.5}O_2$. Electrochem. Commun. *60*, 70–73.

30. Lun, Z., Ouyang, B., Kitchaev, D.A., Clément, R.J., Papp, J.K., Balasubramanian, M., Tian, Y., Lei, T., Shi, T., McCloskey, B.D., et al. (2019). Improved cycling performance of Li-excess cation-disordered cathode materials upon fluorine substitution. Adv. Energy Mater. *9*, 1802959.

31. Li, L., Lun, Z., Chen, D., Yue, Y., Tong, W., Chen, G., Ceder, G., and Wang, C. (2021). Fluorination-enhanced surface stability of cation-disordered rocksalt cathodes for Li-ion batteries. Adv. Funct. Mater. *31*, 2101888.

32. Richards, W.D., Dacek, S.T., Kitchaev, D.A., and Ceder, G. (2018). Fluorination of lithium-excess transition metal oxide cathode materials. Adv. Energy Mater. *8*, 1701533.

33. Yabuuchi, N., Takeuchi, M., Komaba, S., Ichikawa, S., Ozaki, T., and Inamasu, T. (2016). Synthesis and electrochemical properties of $Li_{1.3}Nb_{0.3}V_{0.4}O_2$ as a positive electrode material for rechargeable lithium batteries. Chem. Commun. *52*, 2051–2054.

34. Huang, J., Zhong, P., Ha, Y., Kwon, D.-H., Crafton, M.J., Tian, Y., Balasubramanian, M., McCloskey, B.D., Yang, W., and Ceder, G. (2021). Non-topotactic reactions enable high rate capability in Li-rich cathode materials. Nat. Energy *6*, 706–714.

35. Tabuchi, M., Nakashima, A., Shigemura, H., Ado, K., Kobayashi, H., Sakaebe, H., Tatsumi, K., Kageyama, H., Nakamura, T., and Kanno, R. (2003). Fine $Li_{(4-x)/3}Ti_{(2-2x)/3}Fe_xO_2$ ($0.18 \leq x \leq 0.67$) powder with cubic rock-salt structure as a positive electrode material for rechargeable lithium batteries. J. Mater. Chem. *13*, 1747–1757.

36. Li, B., Sougrati, M.T., Rousse, G., Morozov, A.V., Dedryvère, R., Iadecola, A., Senyshyn, A., Zhang, L., Abakumov, A.M., Doublet, M.-L., et al. (2021). Correlating ligand-to-metal charge transfer with voltage hysteresis in a Li-rich rock-salt compound exhibiting anionic redox. Nat. Chem. *13*, 1070–1080.

37. Wolverton, C., and de Fontaine, D. (1994). Cluster expansions of alloy energetics in ternary intermetallics. Phys. Rev. B Condens. Matter *49*, 8627–8642.

38. Sanchez, J.M. (2017). Foundations and practical implementations of the cluster expansion. J. Phase Equilib. Diffus. *38*, 238–251.

39. McGrogan, F.P., Swamy, T., Bishop, S.R., Eggleton, E., Porz, L., Chen, X., Chiang, Y.-M., and Van Vliet, K.J. (2017). Compliant yet brittle mechanical behavior of Li_2S–P_2S_5 lithium-ion-conducting solid electrolyte. Adv. Energy Mater. *7*, 1602011.

40. Nadler, M.R., and Kempier, C.P. (1959). Crystallographic Data 186. Lithium. Anal. Chem. *31*, 2109.

41. Marianetti, C.A., Morgan, D., and Ceder, G. (2001). First-principles investigation of the cooperative Jahn-Teller effect for octahedrally coordinated transition-metal ions. Phys. Rev. B *63*, 224304.

42. Marianetti, C.A., Kotliar, G., and Ceder, G. (2004). Role of hybridization in Na_xCoO_2 and the effect of hydration. Phys. Rev. Lett. *92*, 196405.

43. Aydinol, M.K., Kohan, A.F., Ceder, G., Cho, K., and Joannopoulos, J. (1997). *Ab initio* study of lithium intercalation in metal oxides and metal dichalcogenides. Phys. Rev. B *56*, 1354–1365.

44. Sakurai, Y., Arai, H., Okada, S., and Yamaki, J. (1997). Low temperature synthesis and electrochemical characteristics of $LiFeO_2$ cathodes. J. Power Sources *68*, 711–715.

45. Armstrong, A.R., Tee, D.W., La Mantia, F., Novák, P., and Bruce, P.G. (2008). Synthesis of tetrahedral $LiFeO_2$ and its behavior as a cathode in rechargeable lithium batteries. J. Am. Chem. Soc. *130*, 3554–3559.

46. Hirayama, M., Tomita, H., Kubota, K., and Kanno, R. (2011). Structure and electrode reactions of layered rocksalt $LiFeO_2$ nanoparticles for lithium battery cathode. J. Power Sources *196*, 6809–6814.

47. Kim, S., Ma, X., Ong, S.P., and Ceder, G. (2012). A comparison of destabilization mechanisms of the layered Na_xMO_2 and Li_xMO_2 compounds upon alkali de-intercalation. Phys. Chem. Chem. Phys. *14*, 15571–15578.

48. Lee, J., Kitchaev, D.A., Kwon, D.-H., Lee, C.-W., Papp, J.K., Liu, Y.-S., Lun, Z., Clément, R.J., Shi, T., McCloskey, B.D., et al. (2018). Reversible Mn^{2+}/Mn^{4+} double redox in lithium-excess cathode materials. Nature *556*, 185–190.

49. Chen, R., Ren, S., Knapp, M., Wang, D., Witter, R., Fichtner, M., and Hahn, H. (2015). Disordered lithium-rich oxyfluoride as a stable host enhanced Li+ intercalation storage. Adv. Energy Mater. *5*, 1401814.

50. Kim, J.-H., Myung, S.-T., Yoon, C.S., Kang, S.G., and Sun, Y.-K. (2004). Comparative study of $LiNi_{0.5}Mn_{1.5}O_{4-\delta}$ and $LiNi_{0.5}Mn_{1.5}O_4$ cathodes having two crystallographic structures: Fd3m and P4332. Chem. Mater. *16*, 906–914.

51. Thackeray, M.M., Johnson, P.J., de Picciotto, L.A., Bruce, P.G., and Goodenough, J.B. (1984). Electrochemical extraction of lithium from $LiMn_2O_4$. Mater. Res. Bull. *19*, 179–187.

52. Yang, M., Zhao, X., Yao, C., Kong, Y., Ma, L., and Shen, X. (2016). Nanostructured cation disordered Li_2FeTiO_4/graphene composite as high capacity cathode for lithium-ion batteries. Mater. Technol. *31*, 537–543.

53. Ji, H., Kitchaev, D.A., Lun, Z., Kim, H., Foley, E., Kwon, D.-H., Tian, Y., Balasubramanian, M., Bianchini, M., Cai, Z., et al. (2019). Computational investigation and experimental realization of disordered high-capacity Li-ion cathodes based on Ni redox. Chem. Mater. *31*, 2431–2442.

54. Yu, Z., Qu, X., Wan, T., Dou, A., Zhou, Y., Peng, X., Su, M., Liu, Y., and Chu, D. (2020). Synthesis and mechanism of high structural stability of nickel-rich cathode materials by adjusting Li-excess. ACS Appl. Mater. Interfaces *12*, 40393–40403.

55. Choi, S., and Manthiram, A. (2002). Synthesis and electrochemical properties of $LiCo_2O_4$ spinel cathodes. J. Electrochem. Soc. *149*, A162.

56. Kitchaev, D.A., Lun, Z., Richards, W.D., Ji, H., Clément, R.J., Balasubramanian, M., Kwon, D., Dai, K., Papp, J.K., Lei, T., et al. (2018). Design principles for high transition metal capacity in disordered rocksalt Li-ion cathodes. Energy Environ. Sci. *11*, 2159–2171.

57. Lee, E., Kwon, B.J., Dogan, F., Ren, Y., Croy, J.R., and Thackeray, M.M. (2019). Lithiated spinel $LiCo_{1-x}Al_xO_2$ as a stable zero-strain cathode. ACS Appl. Energy Mater. *2*, 6170–6175.

58. Zhang, W., Seo, D.-H., Chen, T., Wu, L., Topsakal, M., Zhu, Y., Lu, D., Ceder, G., and Wang, F. (2020). Kinetic pathways of ionic transport in fast-charging lithium titanate. Science *367*, 1030–1034.

59. David, W.I.F., Thackeray, M.M., De Picciotto, L.A., and Goodenough, J.B. (1987). Structure refinement of the spinel-related phases $Li_2Mn_2O_4$ and $Li_{0.2}Mn_2O_4$. J. Solid State Chem. *67*, 316–323.

60. Grey, C.P., Yoon, W.-S., Reed, J., and Ceder, G. (2004). Electrochemical activity of Li in the transition-metal sites of O3 $Li[Li_{(1-2x)/3}Mn_{(2-x)/3}Ni_x]O_2$. Electrochem. Solid State Lett. *7*, A290.

61. Bréger, J., Meng, Y.S., Hinuma, Y., Kumar, S., Kang, K., Shao-Horn, Y., Ceder, G., and Grey, C.P. (2006). Effect of high voltage on the structure and electrochemistry of $LiNi_{0.5}Mn_{0.5}O_2$: A joint experimental and theoretical study. Chem. Mater. *18*, 4768–4781.

62. Hoshino, S., Glushenkov, A.M., Ichikawa, S., Ozaki, T., Inamasu, T., and Yabuuchi, N. (2017). Reversible three-electron redox reaction of Mo^{3+}/Mo^{6+} for rechargeable lithium batteries. ACS Energy Lett. *2*, 733–738.

63. Reed, J., and Ceder, G. (2004). Role of electronic structure in the susceptibility of metastable transition-metal oxide structures to transformation. Chem. Rev. *104*, 4513–4533.

64. Kang, K., and Ceder, G. (2006). Factors that affect Li mobility in layered lithium transition metal oxides. Phys. Rev. B *74*, 094105.

65. Reed, J., and Ceder, G. (2002). Charge, potential, and phase stability of layered $Li(Ni_{0.5}Mn_{0.5})O_2$. Electrochem. Solid State Lett. *5*, A145.

66. Lu, Z., MacNeil, D.D., and Dahn, J.R. (2001). Layered cathode materials Li[NixLi(1/3−2x/3) Mn(2/3−x/3)]O2 for lithium-ion batteries. Electrochem. Solid State Lett. *4*, A191.

67. Kang, S.-H., Kim, J., Stoll, M.E., Abraham, D., Sun, Y.K., and Amine, K. (2002). Layered $Li(Ni_{0.5-x}Mn_{0.5-x}M_{2x}')O_2$ (M′=Co, Al, Ti; x=0, 0.025) cathode materials for Li-ion rechargeable batteries. J. Power Sources *112*, 41–48.

68. Yang, X.-Q., McBreen, J., Yoon, W.-S., and Grey, C.P. (2002). Crystal structure changes of $LiMn_{0.5}Ni_{0.5}O_2$ cathode materials during charge and discharge studied by synchrotron based *in situ* XRD. Electrochem. Commun. *4*, 649–654.

69. Ji, H., Wu, J., Cai, Z., Liu, J., Kwon, D.-H., Kim, H., Urban, A., Papp, J.K., Foley, E., Tian, Y., et al. (2020). Ultrahigh power and energy density in partially ordered lithium-ion cathode materials. Nat. Energy *5*, 213–221.

70. Coelho, A.A. (2018). TOPAS and TOPAS-Academic: an optimization program integrating computer algebra and crystallographic objects written in C++. J. Appl. Crystallogr. *51*, 210–218.

71. Tepesch, P.D., Garbulsky, G.D., and Ceder, G. (1995). Model for configurational thermodynamics in ionic systems. Phys. Rev. Lett. *74*, 2272–2275.

72. Carlier, D., Van der Ven, A., Delmas, C., and Ceder, G. (2003). First-principles investigation of phase stability in the O2-$LiCoO_2$ system. Chem. Mater. *15*, 2651–2660.

73. Arroyo y de Dompablo, M.E., Van der Ven, A., and Ceder, G. (2002). First-principles calculations of lithium ordering and phase stability on Li_xNiO_2. Phys. Rev. B *66*, 064112.

74. Ouyang, B., Artrith, N., Lun, Z., Jadidi, Z., Kitchaev, D.A., Ji, H., Urban, A., and Ceder, G. (2020). Effect of fluorination on lithium transport and short-range order in disordered-rocksalt-type lithium-ion battery cathodes. Adv. Energy Mater. *10*, 1903240.

75. Sanchez, J.M., Ducastelle, F., and Gratias, D. (1984). Generalized cluster description of multicomponent systems. Phys. A *128*, 334–350.

76. Nelson, L.J., Hart, G.L.W., Zhou, F., and Ozoliņš, V. (2013). Compressive sensing as a paradigm for building physics models. Phys. Rev. B *87*, 035125.

77. Chib, S., and Greenberg, E. (1995). Understanding the Metropolis-Hastings algorithm. Am. Stat. *49*, 327–335.

78. Kresse, G., and Joubert, D. (1999). From ultrasoft pseudopotentials to the projector augmented-wave method. Phys. Rev. B *59*, 1758–1775.

79. Kresse, G., and Furthmüller, J. (1996). Efficiency of ab-initio total energy calculations for metals and semiconductors using a plane-wave basis set. Comput. Mater. Sci. *6*, 15–50.

80. Tao, J., Tang, H., Patra, A., Bhattarai, P., and Perdew, J.P. (2018). Modeling the physisorption of graphene on metals. Phys. Rev. B *97*, 165403.

81. Tang, H., Chowdhury, S.T.U.R., Tao, J., and Perdew, J.P. (2020). Density functionals combined with van der Waals corrections for graphene adsorbed on layered materials. Phys. Rev. B *101*, 195426.